Computers & Fluids 79 (2013) 140–149

Contents lists available at SciVerse ScienceDirect

Computers & Fluids

journal homepage: www.elsevier.com/locate/compfluid

Influence of two-dimensional smooth humps on linear and non-linear instability of a supersonic boundary layer

Donghun Park, Seung O. Park *

Department of Aerospace Engineering, Room 2311, KAIST, Daejeon 305-701, Republic of Korea

ARTICLE INFO

Article history:
Received 19 December 2012
Received in revised form 28 February 2013
Accepted 27 March 2013
Available online 6 April 2013

Keywords:
Supersonic boundary layer
Stability
Hump
Parabolized stability equations
Oblique breakdown

ABSTRACT

Stability of a supersonic boundary layer over two-dimensional smooth humps with their heights considerably smaller than the local boundary layer thickness is studied by using parabolized stability equations (PSEs). Influence of humps on linear and non-linear evolution of first mode oblique wave in Mach 1.6 boundary layers is investigated. Overall destabilization influence of the hump is confirmed for both linear and non-linear cases. For the case of linear stability, an overall effect of the hump on destabilization is found to be similar to the case of subsonic boundary layer. However, in contrast to the subsonic case, considerable increase of growth rates realized in the fore part of the hump is found to contribute significantly to the overall destabilization in supersonic boundary layer. Oblique breakdown is investigated for the case of non-linear stability study. When compared to the case of flat plate, all the characteristic stages of the oblique breakdown are found to appear at a far more upstream position due to the hump. Results of parametric studies to examine the effect of hump height, location, etc. on stability characteristics are also given. Influence of dip instead of hump is also found to be very significant.

1. Introduction

One important factor affecting boundary layer transition is a surface roughness element. In practical aerodynamic configurations, many types of roughness elements such as humps, waviness, and rivets are often encountered. Since the stability and transition of boundary layer are strongly influenced by surface roughness, the effect of roughness has been studied for a long time. Some of earlier experimental studies provided empirical criteria for transition location with respect to several parameters [1]. Since several experimental studies revealed that transition over roughness is stability governed phenomena [2,3], the boundary layer stability over roughness has received much research attention. The influence of roughness on the boundary layer stability involved in a natural transition scenario was studied first [4]. It is widely known that the initial stage of natural transition process is linear modal growth of instability waves introduced into boundary layer through receptivity process [4]. Thus, theoretical studies have investigated mainly the effect of roughness on the modal growth of the instability waves [5–15].

Recent numerical studies have simulated the flow around an isolated or discrete roughness (three-dimensional) as briefly described in Choudhari et al. [16]. Evidences have been found to elucidate that instability mechanisms other than the modal instability can become significant when roughness is involved. For example, depending on the shape and size of roughness, absolute instability related to vortex shedding and wake instability might be possible mechanisms leading to transition [17]. Transient growth also has been known to be a possible instability mechanism related to transition due to distributed roughness [18]. In the presence of roughness elements, we thus see that various instability mechanisms and complex interactions among those can usually be involved in the transition process.

For modal growth of instability wave over a roughness element, most of the previous theoretical studies were based on the linear stability theory (LST) [19] and studies so far were limited to the case of two-dimensional smooth roughness element. Many LST studies including parametric study were carried out to investigate the stability of boundary layer over a smooth hump and backward- or forward-facing step [5–10]. The effects of hump height, length, location, shape, unit Reynolds number, free-stream Mach number, etc. on the predicted transition location based on e^N criterion were also evaluated [11,12]. Wie and Malik [13] and Gao et al. [14] carried out PSE analysis which can account for flow non-parallelism and surface curvature to study the linear stability over surface waviness and a smooth hump, respectively. Destabilizing effect of roughness on the modal growth of the instability waves was confirmed. Wörner et al. [15] also confirmed the destabilization effect by direct numerical simulation (DNS) analysis.

Most of the previous theoretical studies have dealt with the linear stability of subsonic boundary layer over a smooth roughness.

* Corresponding author. Tel.: +82 42 350 3713.
E-mail address: sopark@kaist.ac.kr (S.O. Park).

0045-7930
http://dx.doi.org/10.1016/j.compfluid.2013.03.018

Non-linear stability and/or supersonic boundary layer stability have rarely been studied so far. Recently, present authors [20] theoretically investigated non-linear evolution of instability waves in incompressible boundary layer over a smooth hump by using non-linear parabolized stability equations (PSEs) analysis. Although linear and non-linear stability of boundary layer has been studied recently by using DNS for simple configurations, investigations on the non-linear stability of boundary layer over roughness by DNS are rarely found within the framework of stability study.

In this study, linear and non-linear stability of supersonic boundary layer over a roughness element is investigated based on parabolized stability equations (PSEs) analysis. The influence of roughness on the evolution of instability waves of discrete mode is examined. To focus on convective instability only, a two-dimensional smooth hump with its height smaller than the local boundary layer thickness is chosen as roughness element. The PSE methodology previously used in the study for incompressible boundary layer [20] is extended to the present study of supersonic boundary layer. Mean flow data is obtained from the solution of Parabolized Navier–Stokes (PNS) equations. Effect of hump on the linear evolution of first mode oblique wave is briefly examined. For the case of non-linear stability, oblique breakdown is investigated by non-linear PSE. Influence of hump height and location is discussed. Influence of dip instead of hump is also briefly examined.

2. Method of analysis

Fig. 1 shows the schematic of the hump geometry used in the present study. L^*, b^* and h^* represent respectively the distance from the leading edge of flat plate to the location of the hump center, half width, and height of the hump. The superscript $*$ is used to denote dimensional variables. The Reynolds number Re is defined as $U^*_\infty L^*/\nu^*$ where U^*_∞ is the free-stream velocity.

The geometry of the hump is given by Eq. (1), which is the same with that used in previous studies [5,11,20].

$$y = y^*/L^* = (h^*/L^*)f(t) = hf(t) \tag{1}$$

where

$$t = (x^* - L^*)/b^* = 2(x-1)/b$$

$$f(t) = \begin{cases} ll1 - 3t^2 + 2|t|^3, & \text{if } |t| \leqslant 1 \\ 0, & \text{if } |t| > 1 \end{cases}$$

The 2-D mean flow data of supersonic boundary layer over a hump are obtained by solving PNS equations [21]. The accuracy of PNS solution as basic flow for linear stability analysis of axisymmetric flows was verified by Hejranfar et al. [22]. The non-dimensional governing equations for 2-D compressible flow in conservation-law form are written as

$$\frac{\partial \vec{U}}{\partial t} + \frac{\partial}{\partial x}(\vec{E}_i - \vec{E}_v) + \frac{\partial}{\partial y}(\vec{F}_i - \vec{F}_v) = 0 \tag{2}$$

where $\vec{U}$ is the flow variable vector, $\vec{E}$ and $\vec{F}$ the flux vector in x and y direction, respectively. The subscripts i and v represent inviscid and viscous flux. Application of curvilinear computational coordinate grid transformation and dropping the streamwise (ξ-direction) derivatives of viscous terms yields PNS which can be compactly expressed as

$$\frac{\partial \vec{U}}{\partial t} + \frac{\partial}{\partial \xi}(\overline{E}_i) + \frac{\partial}{\partial \eta}(\overline{F}_i - \overline{F}_v) = 0 \tag{3}$$

where

$$\overline{E}_i = \frac{1}{J}(\xi_x \vec{E}_i + \xi_y \vec{F}_i), \quad \overline{E}_v = 0, \quad \overline{F}_i = \frac{1}{J}(\eta_x \vec{E}_i + \eta_y \vec{F}_i),$$

$$\overline{F}_v = \frac{1}{J}(\eta_x \vec{E}'_v + \eta_y \vec{F}'_v)$$

The primed terms in the above denote the terms in which streamwise viscous terms are dropped. Details of the above equations are readily available in Refs. [21,23]. In this study, the time iterative PNS (TIPNS) scheme of Tannehill et al. [21] is employed. The Steger–Warming splitting scheme [24] is used to split the streamwise flux vector. No-slip and adiabatic wall boundary condition is specified.

A computer code for PNS solution for both 2-D and axisymmetric flows was made and was validated through several typical axisymmetric flow cases given in Refs. [21,23]. Since the iterative PNS scheme has been proved to capture the upstream influence and inviscid–viscous interaction properly, we believe that the boundary layer over a smooth hump with small height can be computed with sufficient accuracy by the PNS scheme. The similarity solution of compressible boundary layer equation is imposed as inflow condition at far upstream of the hump for PNS marching. The similarity solution was obtained from the boundary layer code which is 4th order accurate in surface normal direction following the work of Iyer [25].

As is well known, PSE can take into account the flow non-parallelism and curvature effect. The PSE approach is computationally more efficient than DNS and requires even less computational time than LST since it performs the stability analysis by downstream marching from the initial condition. Further, it also enables us to carry out non-linear stability study. The PSE has widely been used to study linear and non-linear stability of subsonic and supersonic boundary layers over simple geometries. The PSE formulation and solution technique can be found in many Refs. [26–28].

The PSE method of the present study is the same with that of our previous work for incompressible boundary layers over a hump [20]. For brevity, we only give final form of the equations and more details on formulation is referred to Ref. [20]. The PSE can compactly be written as follows:

$$\hat{D}_{mn}\psi_{mn} + \hat{A}_{mn}\frac{\partial \psi_{mn}}{\partial x_1} + \hat{B}_{mn}\frac{\partial \psi_{mn}}{\partial x_2} = \hat{V}_{22,mn}\frac{\partial^2 \psi_{mn}}{\partial x_2^2} + \frac{F_{mn}}{A_{mn}} \tag{4}$$

where

$$\hat{D}_{mn} = -i\omega\overline{\Gamma} + i\alpha_{mn}\overline{A} + in\beta\overline{C} + \overline{D} + \alpha_{mn}^2\overline{V}_{11} + n^2\beta^2\overline{V}_{33} + n\alpha_{mn}\beta\overline{V}_{31} - i\frac{d\alpha_{mn}}{dx_1}\overline{V}_{11}$$

$$\hat{A}_{mn} = \overline{A} - i2\alpha_{mn}\overline{V}_{11} - in\beta\overline{V}_{31} \quad \hat{B}_{mn} = \overline{B} - i\alpha_{mn}\overline{V}_{12} - in\beta\overline{V}_{23}$$

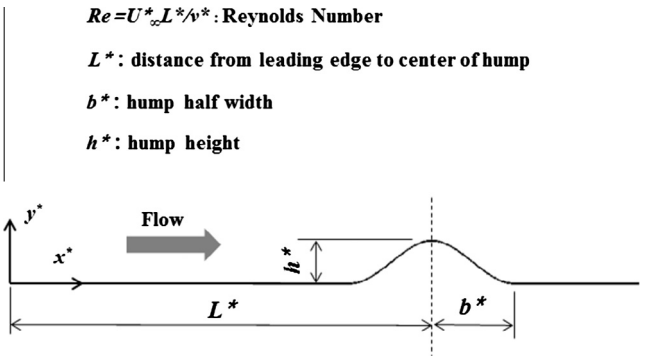

Fig. 1. Schematic of hump geometry.

$$\hat{V}_{22,mn} = \bar{V}_{22} \quad A_{mn} = \exp\left[i\int_{x_{1,0}}^{x_1} \alpha_{mn}(\bar{x}_1)d\bar{x}_1\right]$$

$$F^n(x_1,x_2,x_3,t) = \sum_{m=-M}^{M}\sum_{n=-N}^{N} F_{mn}(x_1,x_2)e^{i(n\beta x_3 - m\omega t)}$$

Here, β and ω are fundamental spanwise wave number and fundamental frequency of disturbance, respectively. The subscripts m and n represent the temporal and spanwise mode number of disturbance, respectively. M and N are the number modes kept in the truncated Fourier series for disturbance. The variable α_{mn} is the streamwise wave number for mode (m, n). The shape function, $\psi_{mn} = \left(\hat{p}_{mn}, \hat{u}_{mn}, \hat{v}_{mn}, \hat{w}_{mn}, \hat{T}_{mn}\right)^T$ represents complex amplitude for mode (m, n). Matrices with over-bar in Eq. (4) are of size 5×5 whose elements correspond to linear part of disturbance equations that are composed of mean flow data and fluid properties. F^n represents the sum of all non-linear terms in the disturbance equations and F_{mn} represents the Fourier components of F^n. The x_1, x_2, and x_3 are streamwise, outward from solid surface, and spanwise direction coordinates of generalized coordinate system, respectively.

For discrete modes, Eq. (4) is subjected to Dirichlet boundary condition that the velocity and temperature disturbances vanish at both the solid surface and free-stream boundary except for mean flow distortion (MFD), i.e. mode (0,0). For MFD, Neumann boundary condition for transverse velocity component is used at free-stream boundary to take into account the change of displacement thickness due to non-linear interaction.

An additional condition, known as the normalization condition, is imposed to determine the unique combination of α_{mn} and ψ_{mn} which satisfy the basic assumptions of PSE. For this, marching procedure of PSE involves an iteration procedure to update α at each streamwise location. In this study, α is updated based on integrated disturbance kinetic energy as given in [27,28].

To solve linear and non-linear PSE numerically, computational grid transformation is introduced. Fourth-order central differencing scheme is used for all the derivatives except for the streamwise derivative of shape function for which second order backward difference scheme is adopted. To efficiently alleviate the numerical instability caused by the weak ellipticity of PSE [29], we follow Chang et al. [27] and Chang [28] which suppress the term corresponding to the streamwise derivative of pressure shape function, i.e., $\partial\hat{p}/\partial x_1$ by weighting the factor in terms of local Mach number. The non-linear terms for non-linear stability are simply treated explicitly as source term. At each iteration, the non-linear term F^n is evaluated in the physical space and is then transformed back into spectral domain by using two dimensional FFT to extract F_{mn}. For the mean flow which is uniform in spanwise direction, the mode symmetry condition can be derived from mathematical characteristics of PSE. This mode symmetry condition results in the reduction of computational cost and memory size since only the quarter of the modes are needed to be kept and analyzed.

To initiate the marching procedure, initial condition which satisfies locally the stability equation is needed. The initial condition is obtained by solving the eigenvalue problem which is almost similar but not identical to LST due to the inclusion of non-parallel terms in the formulation. Since the spatial stability is concerned in the present study, the non-linear eigenvalue problem for the initial condition is formulated and is solved as described in [30].

We note here that PSE is based on the inherent assumption of slow variation in streamwise direction. To ensure, in the present study, slow variation in streamwise direction as much as possible, we consider cases of smooth hump with very small height to width ratio (e.g. $h/b = 0.02$) and whose height is much smaller than the local boundary layer thickness.

3. Results and discussion

In the present study, Mach 1.6 boundary layer ($M_e = 1.6$) of the free-stream unit Reynolds number of 10^7/m with free-stream temperature of 300 K is considered. For both mean flow and stability calculation, Prandtl number and ratio of specific heats are fixed at $Pr = 0.72$ and $\gamma = 1.4$. Two-dimensional smooth humps with rather small height are chosen as roughness element so that no large separation and associated flow unsteadiness are involved.

3.1. Mean flow data

As mentioned above, the mean flow data for stability analysis is obtained from the solution of PNS equations. Since we employ general coordinate system, there is no restriction on the orthogonality of the coordinate system for both PNS calculation and PSE analysis. The x_2 coordinate is in the same direction with that of y coordinate of Cartesian system.

Fig. 2a shows several skin friction coefficient curves from PNS solutions for Mach 1.6 boundary layer for various hump heights. The location of hump center is at $L^* = 0.1$ m corresponding to the Reynolds number 10^6 based on L^* and the hump width is fixed at $b^*/L^* = 0.1$. The streamwise extent of computational domain is

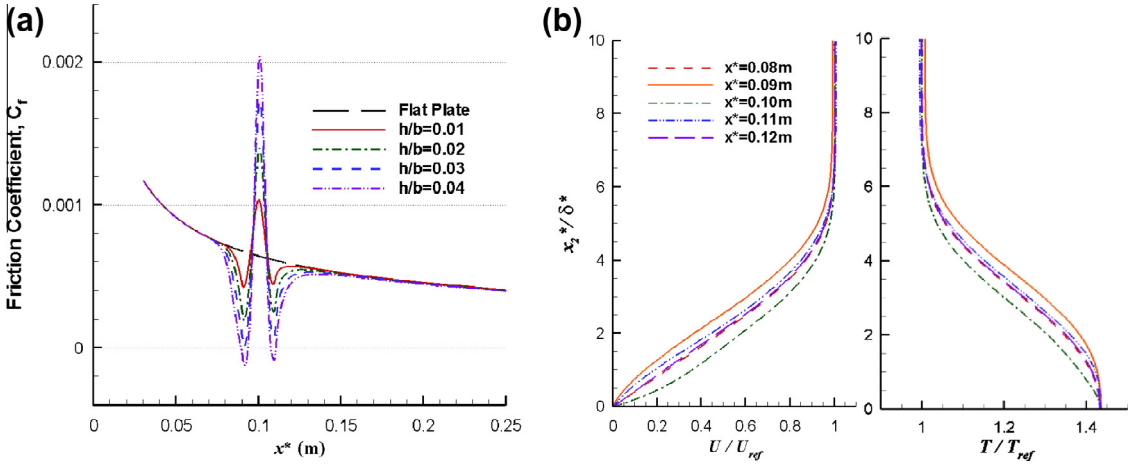

Fig. 2. (a) Typical skin friction coefficient curves and (b) streamwise velocity and temperature profiles at $h/b = 0.02$.

specified such that the locations of inflow and outflow boundary are at $7b^*$ and $23b^*$ away from the hump center, respectively ($0.03\ \text{m} \leqslant x^* \leqslant 0.33\ \text{m}$). The height of the computational domain is set to be 600 times the boundary layer length scale (δ^*) at $x^* = 0.05$ m. Similarity solution of flat plate boundary layer at the inflow boundary is used as inflow condition. For computed results shown in Fig. 2 and 1501 grid points with uniform spacing ($\Delta x^* = 0.002L^*$) in the streamwise direction with 100 grid points over the hump region and 401 grid points in the y-direction with clustering near the surface was used which yielded accurate enough mean flow data.

We see from Fig. 2a that the skin friction around the hump is considerably deviated from that over a flat plate as expected. The skin friction decreases and rises sharply over a fore part of the hump region. It then decreases around the hump center and increases again to asymptotically reach the value of the flat plate boundary layer. As the hump height increases, the deviation of skin friction from that of flat-plate boundary layer naturally becomes greater. In contrast to subsonic cases [5,20,31], we note that the lowest value of the skin friction appears at the upstream of the hump center in supersonic case. This means that a separation would first occur at a location upstream of hump center if the height increases. The boundary layer over the hump becomes incipient to separation at around $h/b = 0.03$ in the present flow condition. We comment here that the peak deviation of skin friction from that of the flat plate in the downstream region of the hump was smaller in this supersonic case than in subsonic flow cases of previous studies. The reason for this discrepancy can be easily explained. In the supersonic flow case, the flow becomes compressed as the hump center is approached while the flow expands beyond the hump center. This expansion accelerates the flow in the downstream of the hump resulting in the increase of skin friction coefficient.

The streamwise velocity and temperature profiles around a hump with $h/b = 0.02$ case are illustrated in Fig. 2b. Although the general tendency of the velocity profile change looks similar to that in subsonic cases, a difference in tendency for supersonic case should be noted. As can be identified from Fig. 2a, streamwise velocity profile is likely to change into the inflectional type profile ahead of the hump for supersonic case, which is of course due to the adverse pressure gradient in this region. Then, the velocity profile becomes fuller as the center of the hump is approached and again the profile becomes less full after passing the center. Beyond the hump region, the velocity profile eventually adapts to the flat plate profile.

3.2. Linear stability

The reference length scale in the stability analysis is a boundary layer length scale δ^* which is defined as $\delta^* = x^*/\sqrt{\text{Re}_{x^*}}$. The Reynolds number based on this length scale, R, is defined as $R = U_\infty^*\delta^*/\nu^* = \sqrt{\text{Re}_{x^*}}$. The non-dimensional frequency F is defined by

$$F = \frac{2\pi f^* \nu_e^*}{(U_e^*)^2} \times 10^6 \tag{5}$$

The present PSE code is first validated for stability analysis for supersonic flat plate boundary layers. Following the calculations of Chang et al. [27], linear PSE analyses were carried out for $F = 112$ and 220 disturbance at $M_e = 1.6$ and 4.5 boundary layer, respectively. For non-linear cases, oblique breakdown for $M_e = 2$ and non-linear evolution of Mack's second mode for $M_e = 4.5$ boundary layer were carried out as in Chang [28]. All the results obtained showed very good agreement with the reference data to ensure the accuracy of the present code.

For the stability calculation of the present study, the grid distribution in y-direction is chosen differently from that for the mean flow calculation. The mean flow data at stability grid points were obtained by interpolation of those from the PNS calculation illustrated in Fig. 2. Test calculations were carried out with various grid distributions for stability analysis with the same mean flow data to confirm that the interpolation of the mean flow data does not affect the stability results. Through this test calculations, we chose 201 grid points within $200\delta^*$ or $250\delta^*$ in x_2-direction with clustering near the solid boundary for stability analysis.

We now present the results of PSE analyses for the linear evolution of instability waves in $M_e = 1.6$ boundary layer over the hump located at $L^* = 0.1$ m with $b^*/L^* = 0.1$ and $h^*/b^* = 0.02$. The hump height is approximately 34.2% of the local flat plate boundary layer thickness at $L^* = 0.1$ m ($\delta_{99}^* \approx 0.000585$ m). The locations of the start, the center, and the end of the hump correspond to $R \approx 948.7$, $R = 1000$, and $R \approx 1048.8$, respectively. It is well-known from LST that the oblique wave is more unstable than 2-D wave having the same frequency for supersonic boundary layers of edge Mach number less than about 4. Fig. 3a shows the growth rate curve of the oblique wave with $F = 20$ and $\beta/R \times 10^4 = 0.83$ together with the curve for the flat plate case. The neutral point of lower branch is at around $R = 670$. Throughout the present study, growth rates (σ) are based on integrated disturbance kinetic energy which is defined by

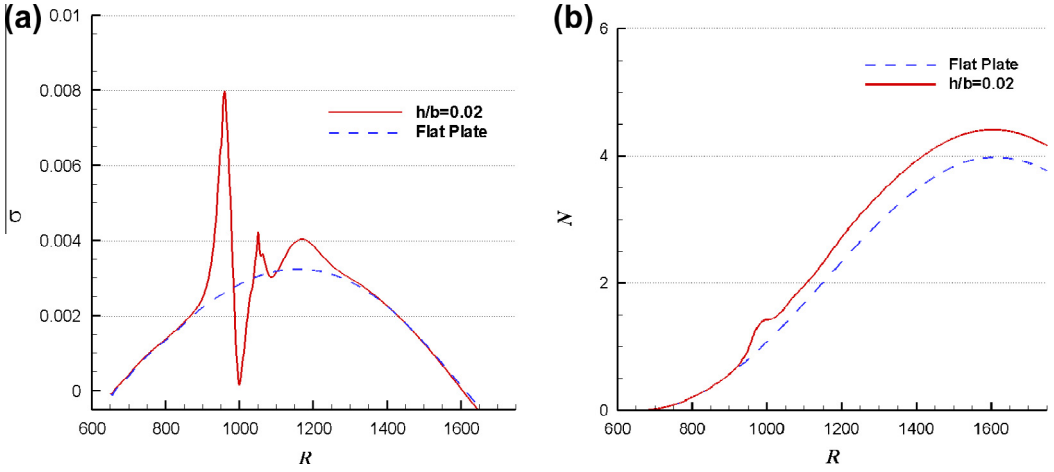

Fig. 3. (a) Growth rate and (b) N-factor curves for $F = 20$ and $\beta/R \times 10^4 = 0.83$.

$$\sigma = -\mathrm{Im}(\alpha) + \mathrm{Re}\left[\frac{\int_0^\infty \bar{\rho}\left(\hat{u}^\dagger \frac{\partial \hat{u}}{\partial x_1} + \hat{v}^\dagger \frac{\partial \hat{v}}{\partial x_1} + \hat{w}^\dagger \frac{\partial \hat{w}}{\partial x_1}\right) dx_2}{\int_0^\infty (\hat{u}^\dagger \hat{u} + \hat{v}^\dagger \hat{v} + \hat{w}^\dagger \hat{w}) dx_2}\right] \quad (6)$$

where superscript † denotes complex conjugate.

We see from Fig. 3a that the growth rate over a hump deviates very much, as expected, from that of the flat plate case. The instability wave undergoes abrupt destabilization, stabilization, and destabilization as it passes the hump. It can be inferred from the skin friction curves and velocity profiles shown in Fig. 2a and b that the steep change of growth rate is a direct reflection of the mean flow modification owing to the hump. The largest destabilization is seen to occur at upstream of the hump center followed by a stabilized region around the hump center and then milder destabilized region follows. We comment here, for subsonic cases, that the strongest destabilization was observed in the downstream region of the hump center [20]. Thus, one of the major differences between supersonic and subsonic cases would be the location of the strongest destabilization. The greatest destabilization in the region upstream of the hump center is consistent with occurrence of the smallest skin friction associated with inflectional velocity profile as illustrated in Fig. 2a and b. The transient behavior is a well-known inherent characteristic of PSE analysis. This refers to an abrupt variation of stability property over a short streamwise distance reflecting a critical change of the mean flow. The transient behavior of PSE solution represented by the wiggling of the growth rate curve was discussed in our previous work [20] on stability study over a hump in subsonic flow case. The wiggling in the growth rate curve of Fig. 2a also represents the consequence of this transient behavior. We comment here that, as given in [20], overall destabilization of disturbance amplitude of linear evolution obtained from PSE analysis for a smooth hump in incompressible boundary layer case was in good agreement with DNS result [32] for an elliptic hump having the same height to width ratio with studied smooth hump.

N-factor which represents logarithmic measure of amplification was computed by integrating growth rates along streamwise coordinate and is plotted in Fig. 3b. We easily see that overall effect of hump is destabilization of instability waves as expected. Fig. 3 indicates that major contribution to overall destabilization originates in the region upstream of the hump center. In contrast to incompressible flow cases the destabilization effect in the region beyond the hump center is rather weak in supersonic case.

Fig. 4a shows *N*-factor curves of the oblique wave of $F = 20$ and $\beta/R \times 10^4 = 0.83$ for the cases of several hump heights with location and width fixed ($L^* = 0.1$ m and $b^*/L^* = 0.1$). Hump heights in terms of boundary layer thickness are 17.1%, 34.2%, 51.3%, and 68.4% for $h/b = 0.01$, 0.02, 0.03, and 0.04, respectively. We obviously see that overall destabilization increases with hump height as expected. The similar behavior was observed in the previous studies for incompressible cases [5,11,20]. We note that the maximum *N* value is not linearly proportional to the hump height. Since the mean flow modification becomes greater with hump height, we easily conjecture that the mean flow modification might have contributed a lot to result in larger growth rate.

Fig. 4b compares *N*-factor curves for the cases of several streamwise hump locations of a fixed configuration ($b^* = 0.01$ m and $h^*/b^* = 0.02$). Hump locations of $L^* = 0.1$, 0.125, 0.15, 0.175, and 0.2 m correspond to $R \approx 1000$, 1118, 1225, 1323, and 1414, respectively. At these locations, the hump height in terms of boundary layer thickness varies as 34.2%, 30.6%, 27.9%, 25.8%, and 24.2%. This may suggest that the destabilization due to hump is likely to become weaker as the hump location moves downstream. However, we find from Fig. 4b that *N*-factor curves show almost the same overall destabilization effect for the cases of hump locations up to $L^* = 0.175$ m. The overall destabilization is seen to decrease beyond $L^* = 0.2$ m. A closer look on the curves confirms us that the maximum value of *N* does not monotonically decrease with hump location. We see that the maximum values of *N* are almost the same when $0.125\ \mathrm{m} \leqslant L^* \leqslant 0.175$ m. In fact, the maximum values for $L^* = 0.125$, 0.150, and 0.175 m cases were found to be 4.475, 4.497, and 4.476, respectively. Although the differences are very small, the highest *N* value is obtained for the case of $L^* = 0.15$ m ($R \approx 1225$). The location of $R \approx 1225$ corresponds to the location of maximum growth rate for the flat plate case (see Fig. 3a). This implies that the overall destabilization due to hump depends not only on the degree of mean flow modification but also on the relative location of the hump with respect to unstable region of the instability wave of the flat plate case. To examine this further, we carried out additional calculations for the cases of various hump height that gives the same ratio of the hump height to boundary layer thickness at several streamwise locations of Fig. 4b. We found that overall destabilization was most pronounced for the case of hump at $L^* = 0.15$ m. Thus, we conjecture that the largest linear overall destabilization is expected for the hump located at around the most unstable region of the instability wave for the flat plate case. Recalling that the unstable region of an instability wave varies with the wave frequency, we conjecture that the hump location of the largest destabilization should also depend on the wave frequency.

When compared to the incompressible case [20], we found that overall destabilization effect in terms of *N*-factor was reduced a bit in supersonic case for the same ratio of the hump height to boundary layer thickness.

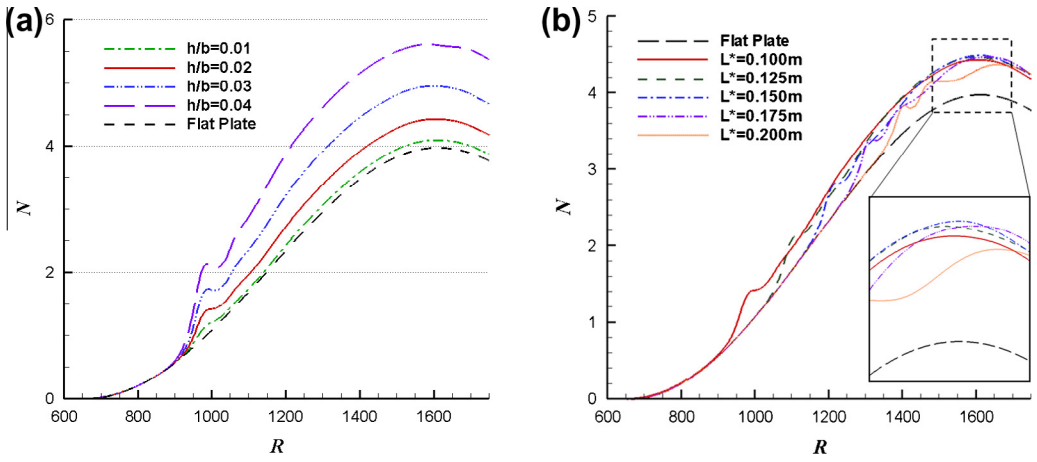

Fig. 4. *N*-factor curves for (a) several hump heights and (b) several hump locations.

3.3. Non-linear stability – oblique breakdown

The oblique transition [33–36] in a supersonic boundary layer has gained much attention since oblique wave is most unstable in supersonic boundary layers. As is well accepted, the oblique breakdown results from non-linear interaction of a pair of oblique waves. Previous studies have confirmed that results from non-linear PSE analysis for oblique breakdown process are in very good agreement with those of DNS up to the region ahead of final breakdown stage [33,36]. Previous studies have carried out PSE analysis for oblique breakdown mainly for flat plate boundary layer case. In this study, PSE analyses are done to evaluate the influence of hump on oblique breakdown process. A pair of oblique waves obtained from local stability analysis is prescribed as initial condition in the region upstream of hump. Non-linear evolution initiated by the oblique waves is analyzed by non-linear PSE analysis. Throughout the present study, five modes are kept in the analysis for both temporal mode and spanwise spatial mode ($M = 5$, $N = 5$).

A pair of oblique wave with $F = 20$ and $\beta/R \times 10^4 = \pm 0.83$ is imposed at $R = 751$ as fundamental mode $(1,\pm1)$ with the maximum rms amplitude of $A_0 = 0.1\%$. The case of the hump located at $L^* = 0.1$ m ($R = 1000$) with $b^*/L^* = 0.1$, and $h^*/b^* = 0.02$ is considered first. Fig. 5a shows the evolution of maximum amplitude of u-velocity disturbances. Amplitudes of several modes are plotted again in Fig. 5b together with those for a flat plate case. The vertical dashed lines indicate the start and end location of the hump geometry. The results for the flat plate case exhibit typical characteristics of oblique breakdown process as already observed in previous studies [35,36].

We see from Fig. 5a and b that (0,2) mode is highly amplified while the fundamental mode almost follows the linear evolution. The (0,2) mode represents the stationary mode whose spanwise wave length is half of that of the fundamental mode. It is generated via non-linear interaction of the fundamental mode. As well known from previous studies for boundary layer and plane channel cases, this mode corresponds to the streamwise vortices and streamwise streaks. The amplitude of this mode overtakes that of the fundamental mode and becomes the mode of the highest amplitude. In addition to (0,2) mode, other modes such as mean flow distortion (MFD) [(0,0)] and (2,2) modes are also highly amplified. We see that all modes are largely amplified further downstream which may eventually result in breakdown. PSE calculation no longer works to get converged solution and calculation terminates at $R = 1425$ and $R = 1489$ for the hump and the flat plate case, respectively. It was observed that the present non-linear PSE marching could not proceed further when the largest amplitude reached around 10%. Keeping only a finite number of Fourier modes might not be sufficient to deal with the situation where all modes are largely amplified. Although numerical failure does not directly imply the breakdown stage, it can be regarded as a good indicator of a beginning of breakdown process.

Fig. 5b illustrates that disturbance amplitudes in the hump case start to deviate from those for a flat plate case from the beginning of the hump region. Naturally, amplitudes of all the modes gain higher magnitude beyond the hump. From Fig. 5b, the streamwise location at which mode (0,2) is seen to exceed fundamental mode amplitude moves upstream by $\Delta R \approx 40$ (from $R \approx 1365$ to $R \approx 1325$) when the hump is present. The amplitude of mode (0,2) reaches 8% at $R \approx 1411$ which is at upstream of the corresponding location for the flat plate case ($R \approx 1478$). Results of Fig. 5a and b indicates clearly that the hump accelerates oblique breakdown process.

Fig. 6 compares contours of instantaneous u-velocity and the disturbance u' in (x_1, x_3)-plane at $x_2^* = 2.28\delta^*$ for the cases of flat plate with and without hump. The Reynolds number coordinate (R) is given additionally to enable easier comparison with Fig. 5. The x_3-coordinate of the figure, enlarged much for better illustration, covers three-spanwise wave length of fundamental mode, $3\lambda_z$ ($\lambda_z = 2\pi/\beta \approx 100.8$). The coordinates (x_1, x_3) are non-dimensionalized by the boundary layer length scale at initial location ($\delta_0^* = \delta^*$ at $R = 751$). The locations of the beginning and the end of the hump correspond to $x_1 \approx 1198.4$ and 1464.7, respectively. Typical characteristics found by Chang and Malik [36] are confirmed in the present result for the flat plate case. In the starting region, we clearly see a pattern resembling checker board due to a pair of oblique waves. Streamwise streaks are then formed and become dominant as the waves proceed downstream. Further downstream, a more complex structure emerges due to amplifications of higher modes. We see that the streaky structure contains two fast and two slow velocity regions appearing alternatively within one spanwise wave length of the fundamental mode. We have confirmed that contours of the stationary modes (time-independent) alone almost coincide with those of all the stationary and non-stationary modes plotted together. This implies that the stationary modes govern the streaky structure. These observations suggest that the streaky structure is a typical characteristic of (0,2) mode. This agrees with the dominance of (0,2) mode over the other modes shown in Fig. 5.

We readily observe that the location of emergence of streamwise streaks shifts upstream owing to the hump. In (x_1, x_3)-plane at $x_2^* = 2.28\delta^*$, the checker board pattern due to disturbances is hardly discernible in the region of the hump since variation of mean flow is much larger than that of the disturbances. Fig. 6b shows contours of disturbance only to present deviation from the

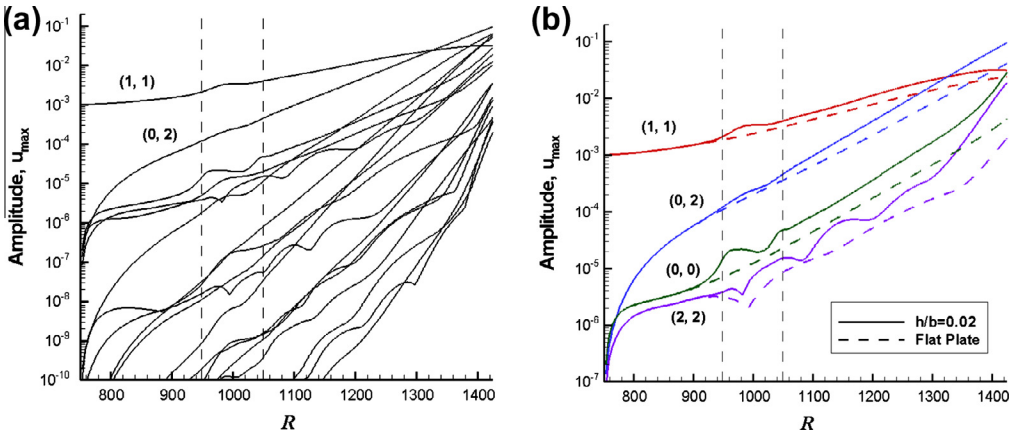

Fig. 5. Maximum amplitudes of u-velocity for (a) all Fourier modes and (b) several modes.

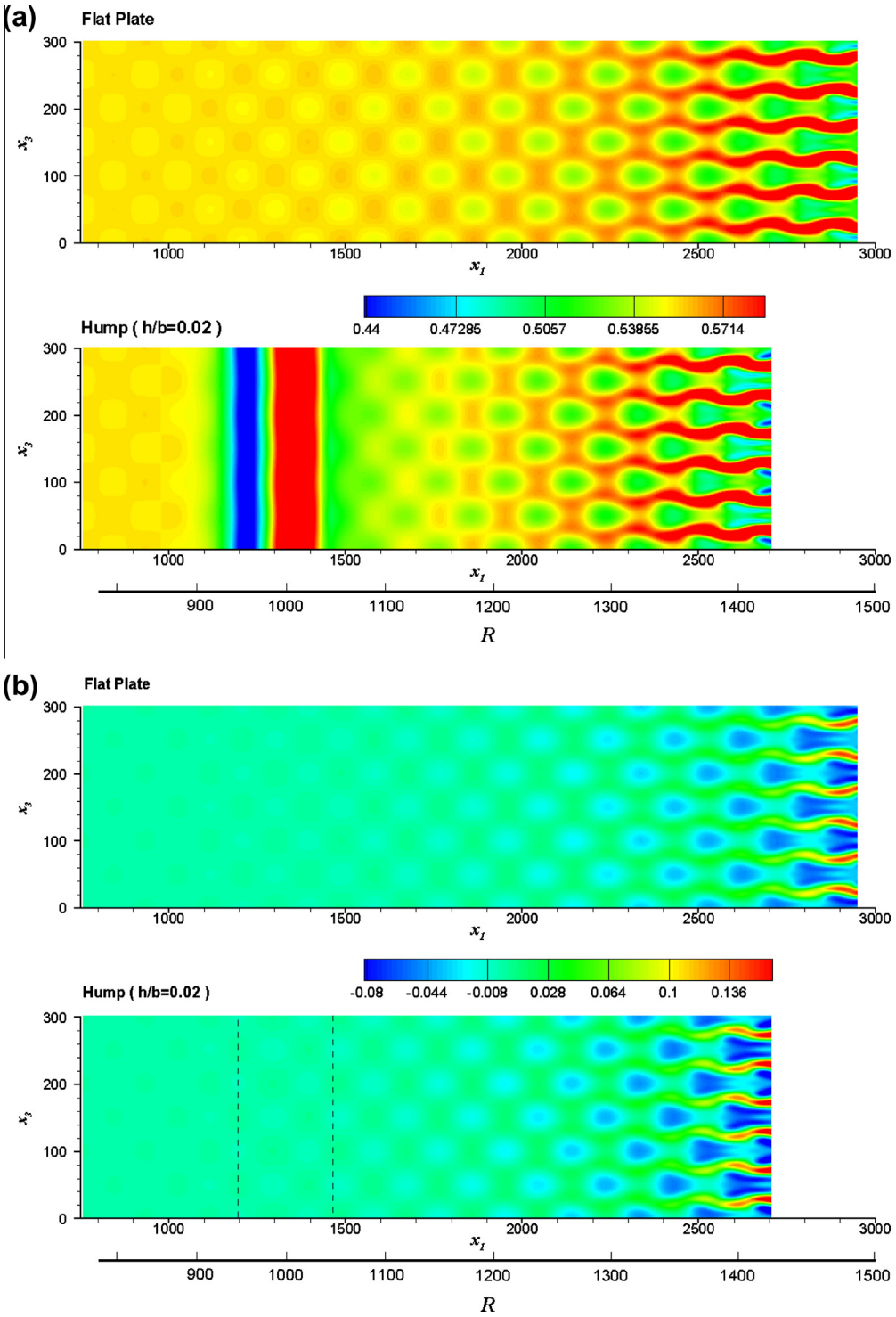

Fig. 6. Contours of instantaneous (a) u-velocity and (b) u' disturbance in (x_1, x_3)-plane at $x_2^* = 2.28\delta^*$.

mean flow for each case. The vertical dashed lines in the figure indicate the start and end location of the hump. As already observed from Fig. 5, comparison of both cases clearly illustrates the overall enhancement of disturbance field due to the hump.

Fig. 7 shows the spanwise vorticity contours in the valley plane ($z = x_3 = 0$). For better illustration, y-coordinate is substantially magnified in the figure. The contour lines represent 81 levels between the magnitude of spanwise vorticity 0.01 and 0.4. For the case of flat plate, spanwise vorticity contour exhibits the typical pattern of oblique breakdown as observed in Chang and Malik [35]. Large spanwise vorticity of mean flow is seen to be concentrated around the hump, which indicates clearly that the development of spanwise vorticity is also enhanced much by the hump. We also see that the location of the same level of vorticity magnitude shifts upstream. Although not shown here, from streamwise vorticity contour and velocity contour in (x_2, x_3)-plane, we also found that (0,2) mode represents not only the streamwise streaks but also counter-rotating streamwise vortices. The streamwise vortices were seen to become strengthened and moved away from the surface with downstream distance.

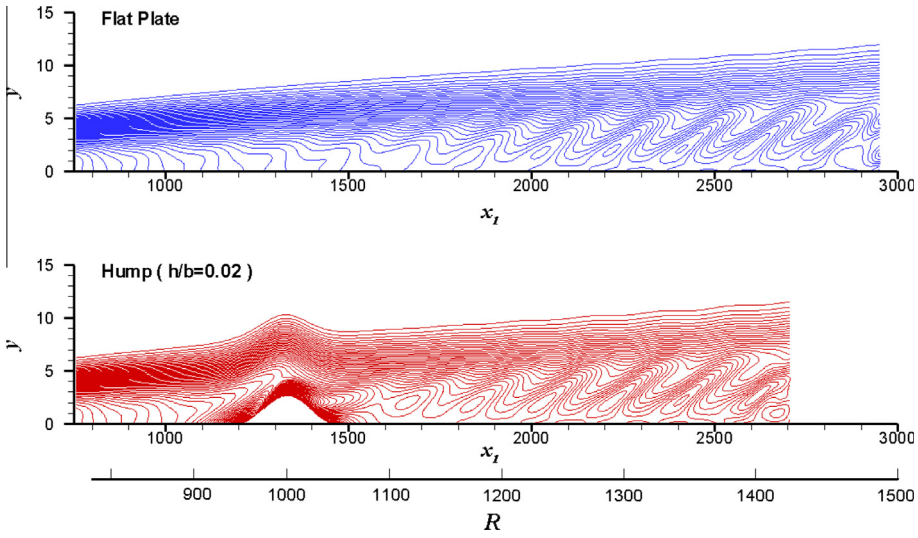

Fig. 7. Spanwise vorticity contours at valley plane.

Fig. 8a shows amplitude evolution of (1,1), (0,2) modes and MFD for several hump heights ($L^* = 0.1$ m, $b^*/L^* = 0.1$). We see from Fig. 8a that the influence of height on oblique breakdown process is similar to that for linear evolution of instability wave. Overall amplification of Fourier modes becomes higher with the hump height. The amplification rate beyond the hump region also appears to increase with height. It is easily expected that larger hump height will lead to earlier breakdown. The amplitude curves for several hump locations are plotted in Fig. 8b. The width and height of the hump were fixed at $b^* = 0.01$ m and $h^*/b^* = 0.02$. We see from the figure that the total amplification in the oblique breakdown process monotonically decreases with downstream shifting of the hump location. This is different from the case of linear evolution in the preceding section. For linear cases, we have seen that almost the same level of overall amplification was reached when the hump was located within the unstable region of the flat plate and the hump location for the largest amplification was located at the middle of the unstable region. For the cases of oblique breakdown, in contrast to this, hump located upstream leads to earlier amplification of Fourier modes to induce non-linear interaction. It is easy to see from Fig. 8b that the streamwise extent of non-linear interaction after additional amplification due to the hump becomes greater as the hump moves upstream. Thus, we can infer that the earlier start of non-linear interaction of the amplified modes results in larger overall amplification.

Effect of initial amplitude of fundamental wave was also examined. For the case of $L^* = 0.1$ m, $b^*/L^* = 0.1$, and $h/b = 0.02$, the calculations for three different initial amplitudes of 0.05%, 0.1%, and 0.2% were carried out. All the amplitudes turned out to increase in proportional to the initial amplitude of the fundamental wave. Amplification rate beyond the hump region remained almost the same regardless of the initial amplitude.

3.4. Influence of dip

We briefly evaluate the influence of dip on the linear evolution and oblique breakdown. Fig. 9a and b shows respectively the N-factor curve and the amplitude evolution. The geometry of the dip is the same with the hump upside down. Thus the depth for the case of Fig. 9 is $h/b = -0.02$ ($L^* = 0.1$ m and $b^*/L^* = 0.1$). The frequency and spanwise wave number were also set to be the same with those of the hump case. The results for cases of the hump and the flat plate are plotted together. We see from Fig. 9a and b that stabilization appears first and then destabilization follows for the case of the dip. The overall destabilization effect is seen to be slightly more pronounced for the case of the dip. Results for

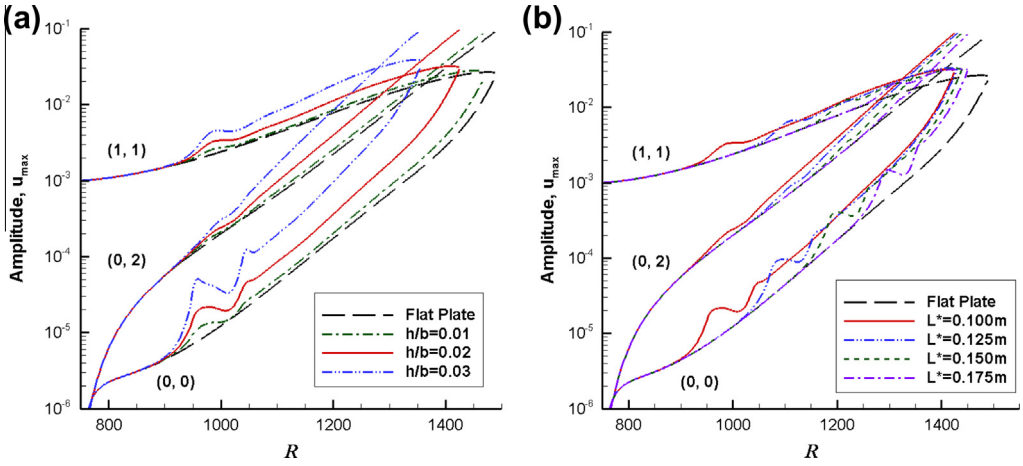

Fig. 8. Maximum amplitudes of (1,1), (0,2) mode and MFD for several hump (a) heights and (b) locations.

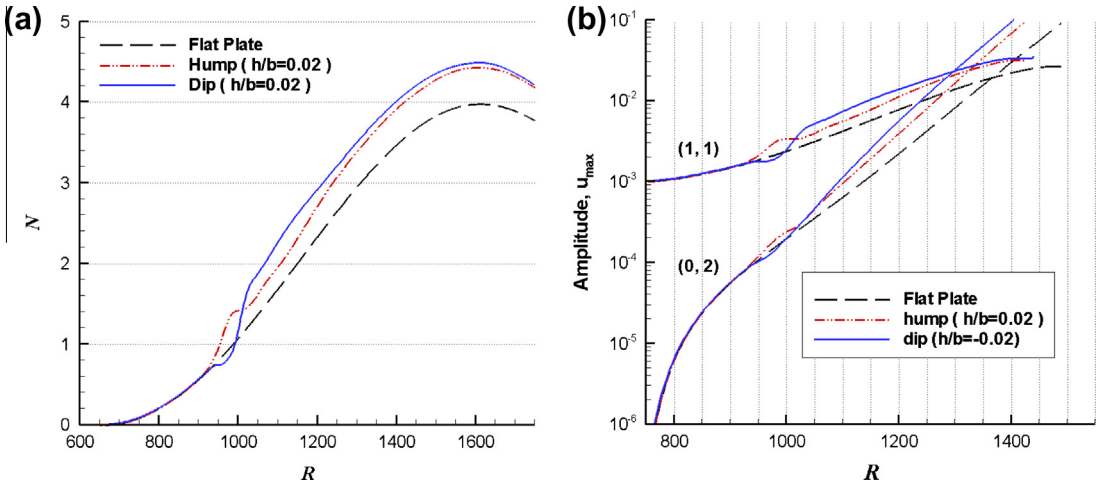

Fig. 9. (a) *N*-factor curve for linear evolution and (b) maximum disturbance amplitudes for oblique breakdown over a dip.

another height case of $h/b = 0.01$ also showed the same trend. This suggests that the dip can also be a dangerous roughness element in the evolution of instability waves in supersonic boundary layers.

4. Concluding remarks

The influence of humps on linear and non-linear instability of a supersonic boundary layer at free-stream Mach number of 1.6 was studied within the framework of PSE analysis. A two-dimensional smooth hump with a height considerably smaller than the boundary layer thickness was considered.

For the case of linear stability, analyses were carried out for the linear evolution of first mode oblique wave. The wave experiences a sequence of destabilization and stabilization as it passes over the hump. An overall effect of the hump on destabilization was similar to the case of subsonic boundary layer. Major difference was in the location where the largest destabilization occurs. In contrast to the subsonic case, considerable increase of growth rates in the fore part of the hump contributed most to the overall destabilization in supersonic boundary layer. The overall destabilization was found to increase non-linearly with the hump height. For a fixed hump height, the overall destabilization effect due to hump location appeared to be almost the same if the hump is located within the unstable region of the instability wave over a flat plate. Although the differences were small, the largest overall destabilization was achieved when the hump was located at the position of the maximum growth rate for the flat plate case. This suggests that relative position of the hump and the unstable region of the given instability wave also affects degree of overall destabilization for the case of linear stability.

For the case of non-linear stability, oblique breakdown was investigated. A pair of first mode oblique wave was imposed at an upstream position of the hump with specified initial amplitude. All the Fourier modes involving the oblique breakdown process were found to be destabilized and attained higher amplitude due to the presence of the hump. When compared to the case of flat plate, all the characteristic stages of the oblique breakdown were found to appear at a more upstream position. Overall amplification of Fourier modes becomes greater with the hump height. As for the hump locations considered (located within the unstable region of flat plate), the overall destabilization of Fourier modes was found to monotonically decrease as the hump position moved downstream.

Influence of dip was also briefly investigated. Effects of the dip on overall destabilization were almost the same with those of the hump for both cases of linear and non-linear stability. The destabilization effect was slightly more intense for the case of the dip.

Acknowledgement

This research was supported by Basic Science Research Program through the National Research Foundation of Korea (NRF) funded by the Ministry of Education, Science and Technology (2010-0012834). For the mean flow calculation, an in-house PNS code developed by Mr. Chang-gwan Lee was used.

References

[1] Fage A. The smallest size of spanwise surface corrugation which affects boundary-layer transition on an airfoil. Aeronaut Res Council, R & M 2120; 1943.
[2] Klebanoff PS, Tidstrom PS. Mechanisms by which a two-dimensional roughness element induces boundary-layer transition. Phys Fluids 1972;15:1173–88.
[3] Dovgal AV, Kozlov VV. Hydrodynamic instability and receptivity of small scale separation regions. In: Arnal D, Michel R, editors. Laminar-turbulent transition. Berlin: Springer-Verlag; 1990. p. 523–31.
[4] Morkovin MV, Reshotko E, Herbert T. Transition in open flow systems: a reassessment. Bull Am Phys Soc 1994;39(9):1–31.
[5] Nayfeh AH, Ragab SA, Al-Maaitah AA. Effect of bulges on the stability of boundary layers. Phys Fluids 1988;31(4):796–806.
[6] Cebeci T, Egan DA. Prediction of transition due to isolated roughness. AIAA J 1989;27(7):870–5.
[7] Ragab SA, Nayfeh AH, Krishna RC. Stability of compressible boundary layers over a smooth backward-facing step. AIAA 90-1449; 1990.
[8] Al-Maaitah AA, Nayfeh AH, Ragab SA. Effect of wall cooling on the stability of compressible subsonic flows over smooth humps and backward-facing steps. Phys Fluids A 1990;2(3):381–9.
[9] Al-Maaitah AA, Nayfeh AH, Ragab SA. Effect of suction on the stability of subsonic flows over smooth backward-facing steps. AIAA J 1990;28(11):1916–24.
[10] Nayfeh AH, Abu-Khajeel HT. Effect of hump on the stability of subsonic boundary layers over an airfoil. Int J Eng Sci 1996;34(6):599–628.
[11] Masad JA, Iyer V. Transition prediction and control in subsonic flow over a hump. Phys Fluids 1994;6(1):313–27.
[12] Masad JA, Malik MR. Link between flow separation and transition onset. AIAA J 1995;33(5):882–7.
[13] Wie YS, Malik MR. Effect of surface waviness on boundary-layer transition in two-dimensional flow. Comput Fluids 1998;27(2):157–81.
[14] Gao B, Park D, Park S. Stability analysis of a boundary layer over a hump using parabolized stability equations. Fluid Dyn Res 2011;43:055503.
[15] Wörner A, Rist U, Wagner S. Humps/steps influence on stability characteristics of two-dimensional laminar boundary layer. AIAA J 2003;31(2):192–7.
[16] Choudhari M, Li F, Chang C-L, Edwards J. On the effects of surface roughness on boundary-layer transition. NASA, Report LF99-8476; 2009.
[17] Chang C-L, Choudhari MM, Li Fei, Venkatachari B. Effect of cavities and protuberances on transition over hypersonic vehicles. AIAA 2011-3245; 2011.
[18] Choudhari M, Fischer P. Roughness-induced transient growth. AIAA 2005-4765; 2005.
[19] Mack LM. Boundary-layer linear stability theory. Special course on stability and transition of laminar flows. AGARD, Report No. 709; 1984.
[20] Park D, Park SO. Linear and non-linear stability analysis of incompressible boundary layer over a hump. Comput Fluids 2013;73:80–96.
[21] Tannehill JC, Miller JH, Lawrence SL. Iterative PNS algorithms for solving 3-D supersonic flows with upstream influences. AIAA 2000-0821; 2000.

[22] Hejranfar K, Esfahanian V, Darian HM. On the use of high-order accurate solutions of PNS schemes as basic flows for stability analysis of hypersonic axisymmetric flows. ASME Trans 2007;129:1328–38.
[23] Tannehill JC, Miller JH, Lawrence SL Development of an iterative PNS code for separated flows. AIAA-99-3361; 1999.
[24] Steger JL, Warming RF. Flux vector splitting of the inviscid gasdynamic equations with application to finite-difference method. J Comput Phys 1981;40(2):263–93.
[25] Iyer V. Computation of three-dimensional compressible boundary layers to fourth-order accuracy on wings and fuselages. NASA CR-4269; 1990.
[26] Herbert T. Parabolized stability equations. Annu Rev Fluid Mech 1997;29:245–83.
[27] Chang C-L, Malik MR, Erlebacher G, Hussaini MY. Linear and nonlinear PSE for compressible boundary layers. NASA CR-191537, ICASE, Report No. 93-70; 1993.
[28] Chang C-L. Langley stability and transition analysis code (LASTRAC) version 1.2 user manual. NASA TM-2004-213233; 2004.
[29] Li F, Malik MR. On the nature of PSE approximation. Theoret Comput Fluid Dyn 1996;8:253–73.
[30] Malik MR. Numerical methods for hypersonic boundary layer stability. J Comput Phys 1990;86:376–413.
[31] Nayfeh AH, Ragab SA, Masad JA. Effect of a bulge on the subharmonic instability of boundary layers. Phys Fluids A 1990;2(6):937–48.
[32] Wörner A, Rist U, Wagner S. Humps/steps influence on stability characteristics of two-dimensional laminar boundary layer. AIAA J 2003; 31(2):192–7.
[33] Joslin RD, Streett CL, Chang C-L. Oblique wave breakdown in an incompressible boundary layer computed by spatial DNS and PSE theory. In: Hussaini MY, Kumar A, Streett CL, editors. Instability, Transition and Turbulence. Springer; 1992. p. 304–10.
[34] Berlin S, Wiegel M, Henningson DS. Numerical and experimental investigations of oblique boundary layer transition. J Fluid Mech 1999;393:23–57.
[35] Chang C-L, Malik MR. Oblique-mode breakdown and secondary instability in supersonic boundary layers. J Fluid Mech 1994;273:323–60.
[36] Mayer CSJ, Fasel HF, Choudhari M, Chang C-L. Detailed comparison of DNS with PSE for oblique breakdown at Mach 3. AIAA 2010-4596; 2010.